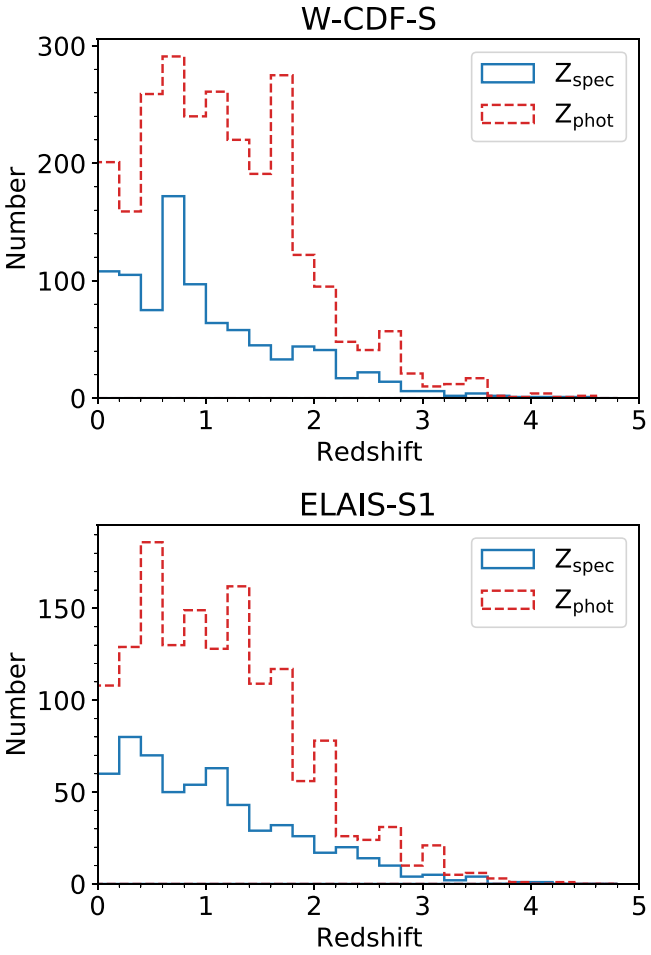

Figure 21. Distributions of the spectroscopic/photometric redshifts of X-ray sources that have spectroscopic/high-quality photometric redshift measurements (see Section 5) in the W-CDF-S and ELAIS-S1 fields, represented by the blue/red histograms.

extinction corrections are applied to the photometry utilized (see Zou et al. 2021 for details).

Photo-zs for X-ray sources that are BL AGNs or non-BL AGNs are derived separately in our work. Here, BL AGNs are identified via classifications from spectroscopic surveys or the SED_BLAGN_FLAG = 1 flag in this work (see Appendix B for details of selecting BL AGN candidates through observed-frame SEDs; sources marked with SED_BLAGN_FLAG = 1 are likely to be BL AGNs). Photo-zs of X-ray sources that are not BL AGNs are provided in Zou et al. (2021) for both the W-CDF-S and ELAIS-S1 fields, which use the default templates of the SED fitting code EAZY (Brammer et al. 2008). In W-CDF-S, 1792 of the matched photo-zs (≈68%) have $Q_z < 1$ (Q_z evaluates the quality of the photo-z; see Equation (8) of Brammer et al. 2008), which are considered to be of high quality. There are 455 sources with both spec-z and $Q_z < 1$ photo-z measurements, which are utilized to assess the reliability of the photo-zs. The normalized median absolute deviation (NMAD) is $\sigma_{\rm NMAD} = 0.04$, and the outlier fraction ($f_{\rm outlier}$, defined as $\Delta z/(1+z_{\rm spec}) > 0.15$; see Zou et al. 2021) is 6.8%; these numbers are similar to the photometric redshift reliability in Chen et al. (2018). The distribution of $en|\Delta z|/(1+z_{\rm spec})$ is given in Figure 22; the distribution of phot-z versus spec-z is also presented in Figure 22. In ELAIS-S1, 1020 ($\approx 65\%$) of the photo-zs have $Q_z < 1$. Among 230 sources with both spec-z and $Q_z < 1$ photo-z measurements, the comparison between spec-z and photo-z produces $\sigma_{\rm NMAD} = 0.03$ and $f_{\rm outlier} = 5.2\%$ (see Figure 22).[50]

For the $\approx 760/430$ SED_BLAGN_FLAG = 1 objects and the $Q_z \geqslant 1$ SED_BLAGN_FLAG = 0.5 objects (sources marked with SED_BLAGN_FLAG = 0.5 are possibly BL AGNs; see Appendix B) in W-CDF-S/ELAIS-S1, we utilized an SED library designed for fitting AGN-dominated sources (Salvato et al. 2009, 2011) with 30 templates in total to estimate the photo-z of these BL AGN candidates with LEPHARE (Arnouts et al. 1999; Ilbert et al. 2006). As the characterization of AGN-dominated sources can be substantially improved when the Lyman break is detected (the optical-to-NIR SED of BL AGNs roughly follows a featureless power law, which may produce large errors for photometric redshifts derived from the template fitting), we match the positions of the optical/NIR counterparts of X-ray sources to the Galaxy Evolution Explorer (GALEX) catalog (Martin et al. 2005) with a matching radius of 1″ and utilize the near-UV (NUV) and far-UV (FUV) fluxes when available. This approach allows the Lyman break to be detected at redshifts as low as $z = 0.7$ (when the FUV flux is available) or $z = 1.5$ (when the NUV flux is available). $\chi^2_{\rm red} < 2$ and band number >10 are utilized to select high-quality photo-z estimates (≈74% of them have high-quality photo-z). BL AGNs identified in spectroscopic surveys that have high-resolution (>100) spec-z measurements are utilized to assess the LEPHARE photo-z quality. Among these 174/138 sources in W-CDF-S/ELAIS-S1, 130/102 have high-quality LEPHARE photo-z measurements utilizing the method above. A comparison between these spec-z and photo-z measurements produces $\sigma_{\rm NMAD} \approx 0.07$ and $f_{\rm outlier} \approx 18\%$ for W-CDF-S and $\sigma_{\rm NMAD} \approx 0.06$ and $f_{\rm outlier} \approx 20\%$ for ELAIS-S1 (see Figure 23). However, as noted in Salvato et al. (2009), the photo-z performance deteriorates when a source is fainter in the optical. For the BL AGNs with spec-z measurements, the median i-band mag is ≈20; this brightness is ≈22 for BL AGN candidates without spec-z measurements. In addition, only ≈40% of the SED_BLAGN_FLAG = 1 objects and the $Q_z \geqslant 1$ SED_BLAGN_FLAG = 0.5 objects are matched to GALEX sources; this number is ≈85% for spectroscopically confirmed BL AGNs. Thus, caution is advised when using LEPHARE photo-z measurements for SED_BLAGN_FLAG = 0.5 or 1 sources.

Combining all the information above, we report the high-quality photo-z measurements in the column PHOTOZ_BEST (see Appendix A): $Q_z < 1$ EAZY photo-z measurements are adopted for sources that have SED_BLAGN_FLAG < 1 and are not identified as BL AGNs in spectroscopic surveys (1792 in W-CDF-S and 1020 in ELAIS-S1); high-quality LEPHARE photo-z measurements are adopted for spectroscopically identified BL AGNs, SED_BLAGN_FLAG = 1 objects, and SED_BLAGN_FLAG = 0.5 objects without $Q_z < 1$ EAZY photo-z measurements (738 in W-CDF-S and 460 in ELAIS-S1). The catalog has high-quality photo-z measurements for 1833/1117 X-ray sources in W-CDF-S/ELAIS-S1 without spec-z measurements. The cumulative histogram of the i-band magnitude of X-ray sources with either spec-z measurements or high-quality photo-z measurements is presented in Figure 24.

[50] As stated in Zou et al. (2021), due to the deeper spectroscopic coverage in W-CDF-S compared to ELAIS-S1, the photo-z qualities in W-CDF-S and ELAIS-S1 listed here are not directly comparable.

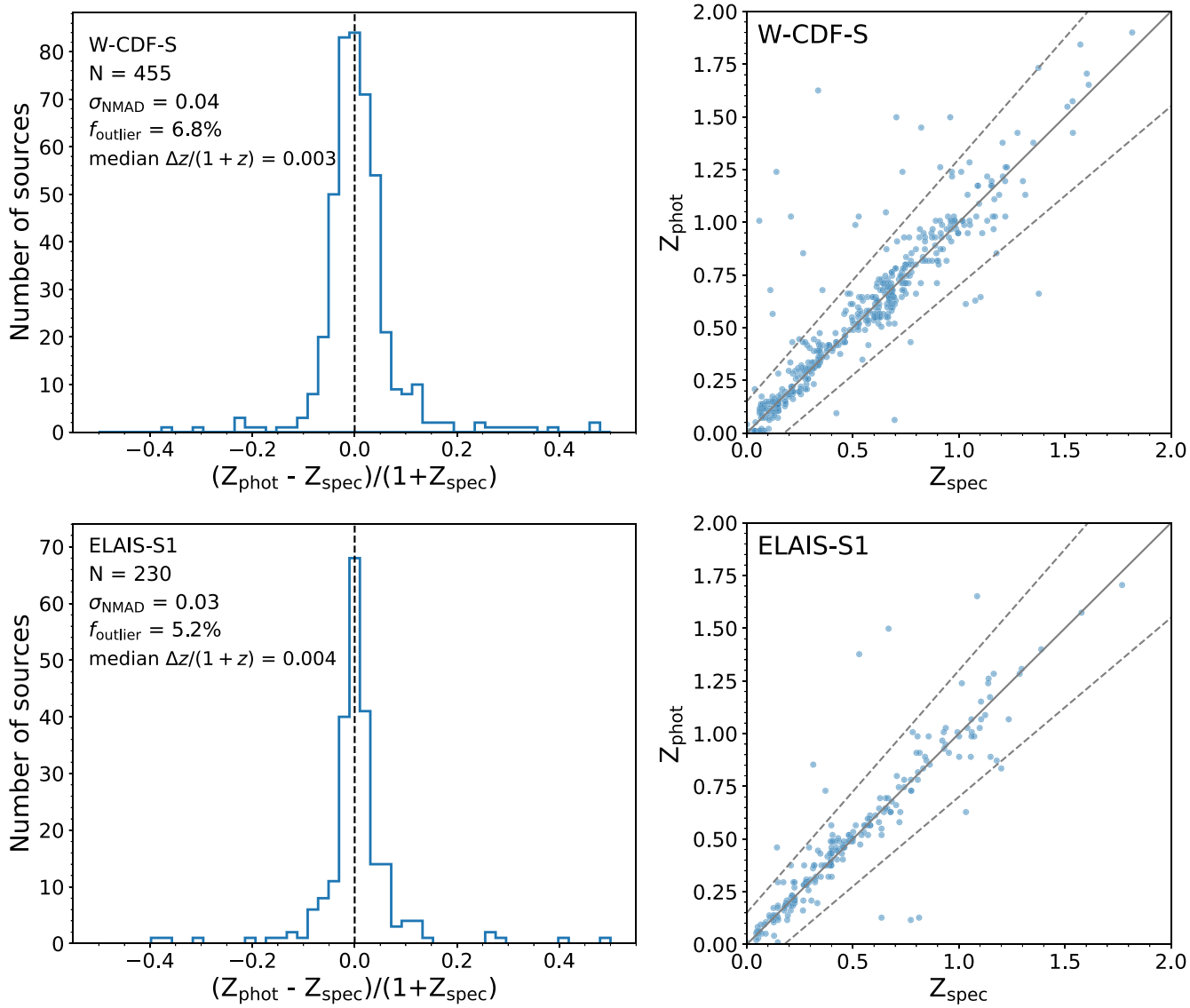

Figure 22. Left: histogram of the fractional difference between the EAZY high-quality photo-zs and the spec-zs. Right: comparison between the EAZY high-quality photo-zs and the spec-zs. The gray solid line represents the $z_{spec} = z_{phot}$ relation; the gray dashed lines represent the $|\Delta z|/(1 + z_{spec}) = 0.15$ boundary.

6. Source Properties and Classification

For the 919/585 X-ray sources with spec-z measurements and 1833/1117 X-ray sources with high-quality EAZY or LEPHARE photo-z measurements (but lacking spec-z measurements) in W-CDF-S/ELAIS-S1, we estimate their X-ray luminosity at rest frame 2–10 keV ($L_{2-10\,keV}$) assuming a power-law spectrum with $\Gamma_{eff} = 1.8$ (which is a typical power-law photon index for AGNs; e.g., Lanzuisi et al. 2013; Yang et al. 2016; Liu et al. 2017) modified by Galactic absorption, utilizing source count rates in the priority order of hard band, full band, and soft band. This prioritization minimizes X-ray absorption effects. Figure 25 displays the distribution of $L_{2-10\,keV}$, as well as the $L_{2-10\,keV}$ versus z distribution. In Figure 26, we show the $L_{2-10\,keV}$ versus z distribution for the whole XMM-SERVS survey and compare it with distributions from selected deep pencil-beam X-ray surveys (CDF-S, Luo et al. 2017; CDF-N, Xue et al. 2016) and shallower X-ray surveys over wider areas (XMM-XXL North, e.g., Menzel et al. 2016; Stripe 82X, e.g., Ananna et al. 2017; LaMassa et al. 2019).[51] While deep pencil-beam surveys can detect less luminous X-ray sources, the AGN sample size provided by the XMM-SERVS survey is substantially larger than the sample size these deep surveys could provide. When compared to shallower X-ray surveys over wider areas, we can see that the XMM-SERVS survey detects a significantly larger number of moderate-luminosity AGNs at log $L_X \sim$42–44; also, due to the superb multiwavelength coverage of XMM-SERVS, the overall number of detected X-ray sources with reliable redshift measurements is larger at all redshifts. The $L_{2-10\,keV}$ versus z coverage of XMM-SERVS is similar to that of the Chandra COSMOS-Legacy survey (e.g., Marchesi et al. 2016), though the Chandra COSMOS-Legacy survey is somewhat deeper: the peak of the log $L_{2-10\,keV}$ distribution of X-ray

[51] We note that for X-ray sources in CDF-S, CDF-N, and Stripe 82X, both spectroscopic redshifts and high-quality photometric redshifts are available, so the sources included in our comparison are those with either spec-z or photo-z; for the XMM-XXL North survey, the sources included are only those with spec-z measurements, due to the lack of available photo-z measurements in this area, currently.

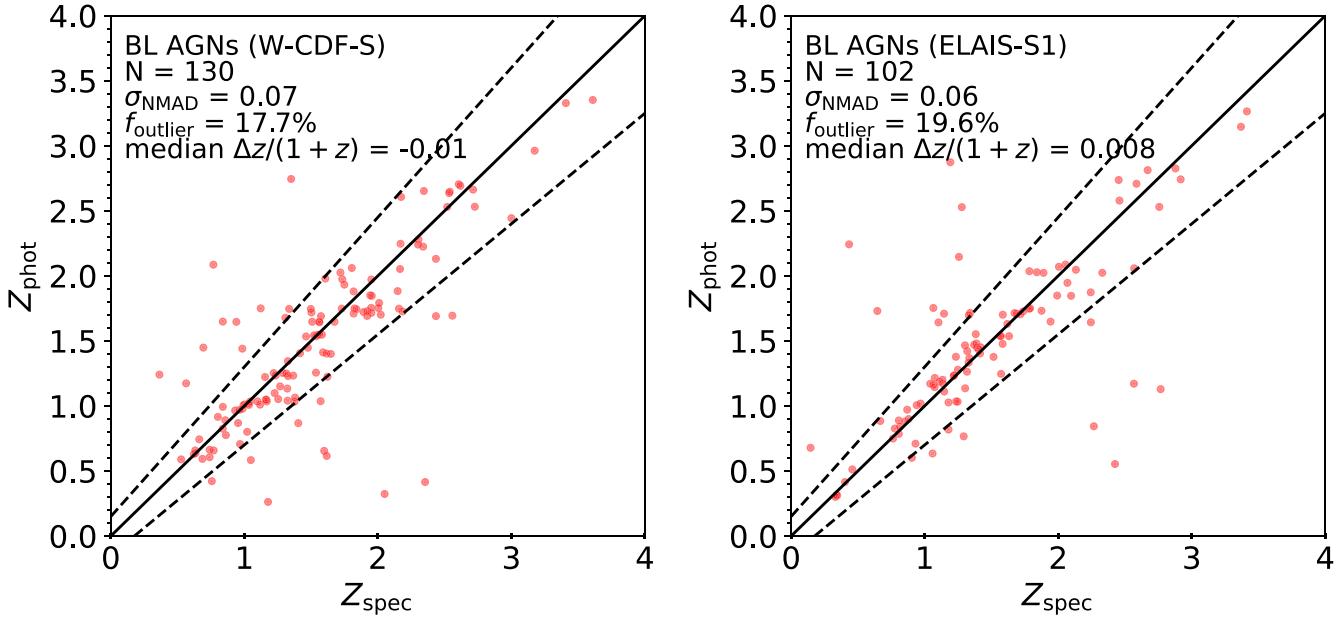

Figure 23. The comparison between the photo-zs and the spec-zs of BL AGNs that have both high-quality photo-z from LEPHARE and resolution > 100 spec-z measurements. The black solid line represents the $z_{spec} = z_{phot}$ relation; the black dashed lines represent the $|\Delta z|/(1 + z_{spec}) = 0.15$ boundary.

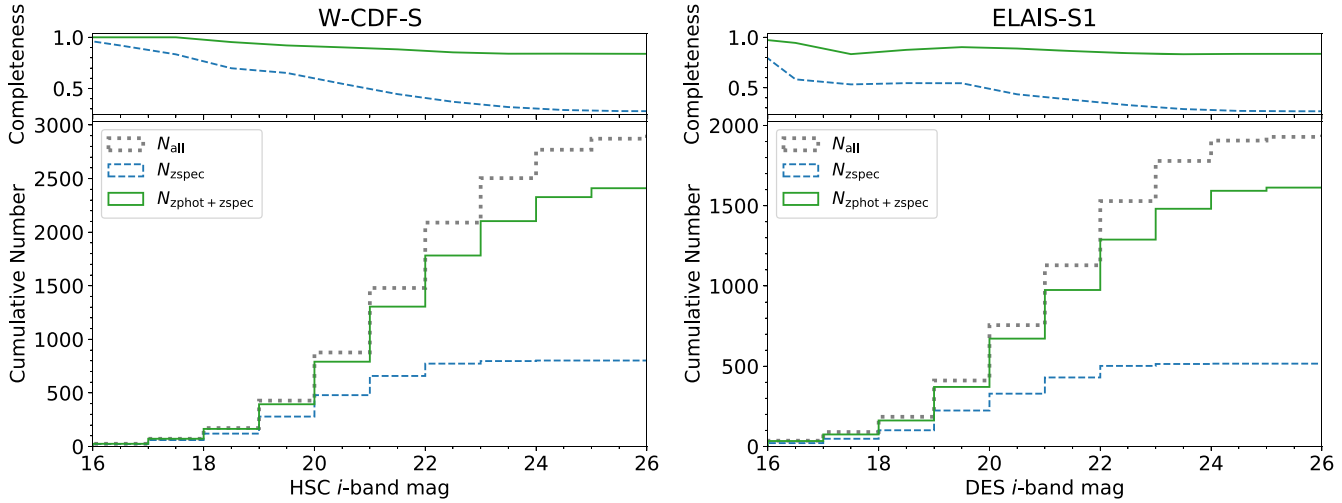

Figure 24. The cumulative distributions of the HSC/DES i-band magnitudes for i-band-detected X-ray sources in W-CDF-S/ELAIS-S1 located within the region with forced photometry (gray dotted histogram), X-ray sources that have spec-z measurements (blue dashed histogram), and X-ray sources that have either spec-z or high-quality photo-z measurements (green solid histogram). The blue dashed/green solid curve in the top panels is the fraction of X-ray sources in the region with forced photometry with spec-z/high-quality photo-z or spec-z measurements as a function of i-band magnitude. Objects without spec-z or high-quality photo-z measurements are SED_BLAGN_FLAG = 0 objects with EAZY $Q_z > 1$ or SED_BLAGN_FLAG > 0 objects with LEPHARE $\chi^2_{red} \geqslant 2$ or band number $\leqslant 10$.

sources in the Chandra COSMOS-Legacy survey is ≈0.5 dex smaller than that of X-ray sources in XMM-SERVS. At the same time, the sample size of AGNs with reliable L_X estimation provided by XMM-SERVS is ≈3 times that of the Chandra COSMOS-Legacy survey.

We also perform basic AGN selection for X-ray sources in our catalogs following criteria from Section 2.3 of Brandt & Alexander (2015) and references therein. The specific criteria utilized are the following:

1. Identified as BL AGNs in spectroscopic surveys (280 AGNs in W-CDF-S; 208 AGNs in ELAIS-S1).
2. Has observed $L_{2-10\,keV} > 3 \times 10^{42}$ erg s^{-1} (in the rest frame) when spec-z measurements or high-quality EAZY or LEPHARE photo-z measurements are available (2337 AGNs in W-CDF-S; 1442 AGNs in ELAIS-S1).
3. Has a power-law effective photon index $\Gamma \leqslant 1$ (412 AGNs in W-CDF-S; 314 AGNs in ELAIS-S1; see Figure 27). This criterion helps select hard X-ray sources that are heavily obscured, which are likely AGNs rather than X-ray binary populations (e.g., Alexander et al. 2005; Brandt & Alexander 2015).
4. Identified as AGNs when utilizing X-CIGALE to perform SED template fitting in Appendix B (2711 AGNs in W-CDF-S; 1696 AGNs in ELAIS-S1). AGNs selected via this SED-based selection method already include AGNs selected from empirical methods that use large X-ray-to-optical or X-ray-to-NIR flux ratios: $\log f_x/f_i > -1$ or $\log f_x/f_{Ks} > -1.2$ (see Figure 28). For the small fraction